frontiers | Frontiers in Materials

ORIGINAL RESEARCH
published: 30 May 2022
doi: 10.3389/fmats.2022.913804

Rational Synthesis of Freestanding $Na_xV_2O_5$-rGO Paper as the Stable Cathode for Sodium Ion Batteries

Qi Wang†, Xin Li†, Junmin Xu, Yueyue Yuan, Xinyue Li and Xinchang Wang*

Key Laboratory of Material Physics of Ministry of Education, School of Physics and Microelectronics, Zhengzhou University, Zhengzhou, China

Flexible $Na_xV_2O_5$/rGO papers were successfully prepared *via* hydrothermal method followed by vacuum filtration as a high-performance cathode for SIBs. The as-prepared $Na_xV_2O_5$/rGO combined flexibility and high conductivity that can buffer stress and facilitate the fast transportation of electrons during the charge-discharge process. As a result, the as-prepared $Na_xV_2O_5$-rGO paper can exhibit a reversible Na-ion storage capacity of ~197 mA h g^{-1} at 100 mA g^{-1} and a good cycling performance with 81% capacity retention for 400 cycles at a high current density of 500 mA g^{-1}, showing great potential in flexible energy storage devices.

Keywords: NaxV2O5/rGO, flexibility, sodium ion batteries, cathode, freestanding

Edited by:
Haibin Tang,
Hefei Institutes of Physical Science (CAS), China

Reviewed by:
Zhengfei Dai,
Xi'an Jiaotong University, China
Hongbo Geng,
Changshu Institute of Technology, China

****Correspondence:***
Junmin Xu
junminxu@zzu.edu.cn

†These authors have contributed equally to this work

Specialty section:
This article was submitted to Semiconducting Materials and Devices, a section of the journal Frontiers in Materials

Received: *06 April 2022*
Accepted: *22 April 2022*
Published: *30 May 2022*

Citation:
Wang Q, Li X, Xu J, Yuan Y, Li X and Wang X (2022) Rational Synthesis of Freestanding $Na_xV_2O_5$-rGO Paper as the Stable Cathode for Sodium Ion Batteries. Front. Mater. 9:913804. doi: 10.3389/fmats.2022.913804

INTRODUCTION

With the increase in environmental concerns, people are eager to search for and develop safe and green energy storage systems (ESS). (Xu et al., 2017; Li et al., 2019). In recent years lithium-ion batteries (LIBs) have been applied to commercial electric vehicles (EVs) and provided a high energy density for large-scale energy storage systems (Xu et al., 2013; Huang et al., 2020), but the costs of lithium and the uneven global distribution of lithium resources gradually restrict their further applications. (Li et al., 2014). Therefore, safe and new cheap ESS that can partially replace LIBs need to be explored (Li et al., 2021). Among the new EES, sodium ion batteries (SIBs) have attracted increasing attention due to the rich potential sources of raw materials and suitable redox potentials (Jiang et al., 2014; Zhao et al., 2020). However, they have approximately 70% larger Na^+ than Li^+, which can bring sluggish diffusion kinetics to the solid state electrode materials, leading to the fast capacity decay and poor rate performance for SIBs (Liang et al., 2018; Huang et al., 2019). Thus, it is necessary to constantly study high-performance cathode materials that can meet the demands of both low cost and good electrochemical performance. (Wang et al., 2020). High-performance electrode materials should have several important traits including good electrical conductivity, abundant electrochemical active sites and desirable structure. (Lu et al., 2016; Pei et al., 2017). The above traits should be considered when designing and preparing high-performance sodium ion batteries.

To date, a large variety of sodium ion conductors such as pyrophosphates (Niu et al., 2019), fluorophosphates (Lim et al., 2014), sulfates (Wu et al., 2014), sodium transition-metal oxides (Liu et al., 2020a), polyanions (Senthilkumar et al., 2020), and the Prussian blue metalates (Liu et al., 2020b; Huang et al., 2021) have been proposed as SIB cathodes. Among these different types of SIB cathode materials, vanadium-based oxides have attracted significant attention due to their high Na-storage capacities, diverse structures, and high electrochemical activity. (Córdoba et al., 2019; Jo et al., 2020). In recent years, a variety of sodium vanadates including V_2O_5 polymorphs (Baddour-Hadjean

et al., 2018), Na_xVO_2 (Guignard et al., 2013), $NaVO_3$ (Venkatesh et al., 2014), NaV_3O_8 (Kang et al., 2015), $Na_{0.33}V_2O_5$ (Shang et al., 2019), and γ-$Na_{0.96}V_2O_5$ (Emery et al., 2018) have been investigated as the SIB cathode materials. Given their good electrochemical performances, people expect to design and prepare high-performance new electrode materials for sodium ion batteries from the various sodium vanadates. More recently, Jingjie Feng et al. reported that $Na_xV_2O_5{\cdot}nH_2O$/KB shows a good electrochemical performance for SIB cathode. A high Na-storage capacity of 239 mAh g^{-1} was acquired at 20 mA g^{-1} and a good discharge capacity retention rate of 91% can be maintained after 90 cycles at 200 mA g^{-1} (Feng et al., 2018). Then, Nicolas Emery et al. reported that the γ-$Na_{0.96}V_2O_5$ cathode material shows a reversible Na^+ insertion/extraction behavior and can deliver a specific capacity of 125 mAh g^{-1} at 0.2°C (Emery et al., 2018). Lately, Yifan Dong et al. studied the NaV_6O_{15} microflowers as an SIB cathode material, which shows a reversible Na-storage capacity of 126 mAh g^{-1}at 100 mA g^{-1}. It also demonstrates good cycle stability and 87% capacity retention over 2000 cycles at 5 A g^{-1} (Dong et al., 2020). These studies inspired us to develop a promising SIBs cathode material by controllable preparation of sodium vanadates with desirable morphology, structure and composition. A one dimensional (1D) structure can reduce ion diffusion path and promote the full use of active sites, which could endow cathode material with enhanced Na-ion storage performance (Zhu et al., 2019). In addition, the high electrochemical performance of $Na_xV_2O_5$ is restricted by its low electron conductivity and large volume change. Design of a composite consisting of 1D $Na_xV_2O_5{\cdot}nH_2O$ nanobelts and conductive carbon is a viable approach, which has both high electrochemical performance and good mechanical properties (Osman et al., 2021). Graphene, as a typical two-dimensional carbon, can provide elastic matrix for loading cathode materials and simultaneously acts as conductive network for strengthening the dynamical process both of electrons and ion transportation (Zhou et al., 2019; Qu et al., 2021). If we can controll fabrication of the 1D $Na_xV_2O_5$ composite with the reduced graphene oxide (rGO), the freestanding $Na_xV_2O_5$/rGO composite cathode with enhanced electrochemical performance would be acquired.

In this work, a freestanding composite (denoted as $Na_xV_2O_5$/rGO) consisting of δ-$Na_xV_2O_5$ nanobelts and rGO was fabricated by a facile hydrothermal method combined with vacuum filtration. The freestanding composite composed of the δ-$Na_xV_2O_5$ nanobelts and rGO offers several advantages. For instance, the bilayered δ-$Na_xV_2O_5$ nanobelts with a large interlayer spacing and 1D belt-shaped morphology can reduce diffusion distance and provide a small diffusion for fast Na^+ ion insertion/extraction reactions (Xu et al., 2020). In addition, the rational introduction of rGO can reduce the aggregation of $Na_xV_2O_5$ nanobelts and improve the conductivity of the whole composite material (Ma et al., 2021), which can strengthen the mechanical integrity of the composite, thus improving the electrochemical performance of the electrode. Besides, compared with the traditional cathodes, the as-prepared freestanding electrode does not use non-conductive binders that can further improve electron transport (Xu et al., 2020). As a result, the as-prepared $Na_xV_2O_5$/rGO electrode could exhibit a Na-storage capacity of ~197 mA h g^{-1} at 100 mA g^{-1} and good cycling performance with 91% of capacity retention after 150 cycles at 100 mA g^{-1}, and high rate performance with ~91 mAh g^{-1} at 500 mA g^{-1}. Moreover, a full Na-ion battery fabricated from the $Na_xV_2O_5$/rGO cathode and hard carbon anode can deliver a Na-storage capacity of 101 mAh g^{-1} at 500 mA g^{-1} and good cycling stability with a capacity retention of >75% over 100 cycles.

EXPERIMENTAL DETAILS

Synthesis of the Ultra-Long $Na_xV_2O_5$ Nanobelts

The $Na_xV_2O_5$ was synthesized by a hydrothermal reaction as follows: 3 mmol of sodiumiodide and 1.5 mmol of vanadium pentoxide were put into the 40 ml of 1 mol/L sodium chloride aqueous solution and constantly stirred for 8 h. The mixture was put into a 40 ml Teflon-lined autoclave and placed into an electric oven at 200°C for 24 h. Finally, the obtained products were washed with deionized water and ethanol serval times and dried at 80°C to obtain $Na_xV_2O_5$.

Synthesis of the Free-Standing $Na_xV_2O_5$/rGO Paper

The free-standing $Na_xV_2O_5$/rGO paper was prepared as follows: 120 mg of the $Na_xV_2O_5$ was synthesized by hydrothermal method and 60 mg of graphene oxide (GO) was synthesized *via* the modified Hummer's method. The mixture of $Na_xV_2O_5$ and GO was ultrasonicated for 2 h followed by constantly stirring overnight until it became homogeneous. The mixed solution of $Na_xV_2O_5$ and GO was put into the Teflon-lined autoclave and placed at 180°C for 24 h. After the hydrothermal reaction, the product was re-dispersed in deionized water and subsequent vacuum filtration. The paper-like product *via* peeling was dried at 80°C for 24 h to obtain the free-standing $Na_xV_2O_5$/rGO composite. The mass loading of the $Na_xV_2O_5$/rGO electrodes is ~3 mg/cm^2.

Electrochemical Measurements

Fabrication of the Sodium Metal- $Na_xV_2O_5$/rGO Half Cell

The $Na_xV_2O_5$/rGO paper was directly cut into a round electrode with a diameter of 1 cm as the cathode and the active mass is ~1.2 mg. The homemade sodium sheets were used both as counter electrodes and reference electrodes. Whatman glass microfiber filters (GF/D) were used as the separator and 1 M $NaClO_4$ in ethylene carbonate (EC): propylene carbonate (PC) (1: 1 by v/v) with 5.0% fluoroethylene carbonate (FEC) as the electrolyte.

Assembly of the Hard Carbon- $Na_xV_2O_5$/rGO Full Cell

The Na-ion full battery was fabricated in an argon-filled glove box composed of $Na_xV_2O_5$/rGO cathode and hard carbon anode**.** The hard carbon anode was prepared by mixing hard carbon, Super P, and polyvinylidene difluoride (8:1:1 wt%) in

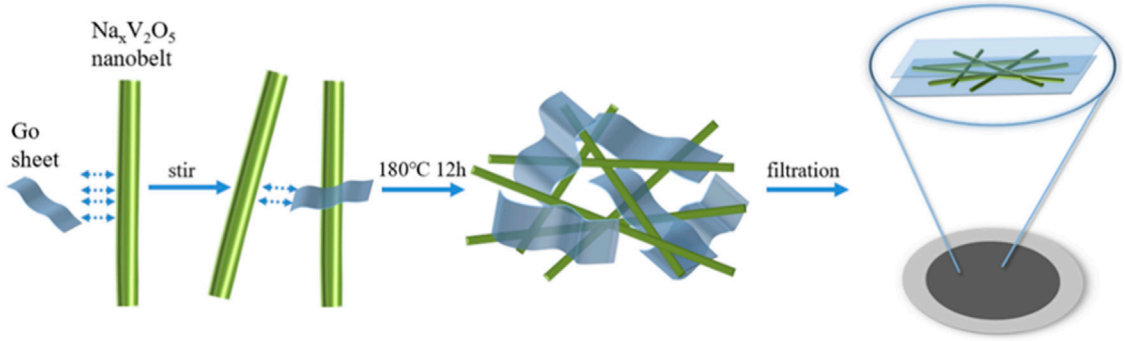

FIGURE 1 | Schematic illustration of the as-prepared $Na_xV_2O_5$/rGO film.

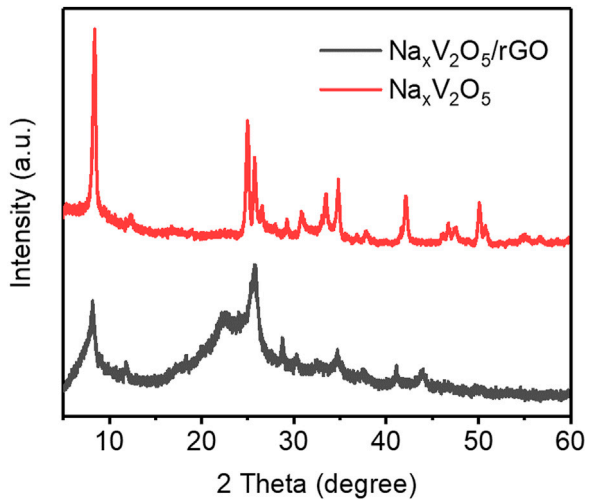

FIGURE 2 | XRD patterns of as-synthesized $Na_xV_2O_5$ powder and $Na_xV_2O_5$/rGO film.

N-Methylpyrrolidone, and then the slurry was spread onto Cu foil. We controlled the negative capacity/positive capacity ratio, which was ~1.1 to guarantee cell balance. The anode was firstly cycled between 0.01 and 1.5 V in a SIB half cell before preparing the full SIB cell.

RESULTS AND DISCUSSION

Figure 1 schematically illustrates the synthesis procedure of the $Na_xV_2O_5$/rGO paper. The mixture of the $Na_xV_2O_5$ and rGO was prepared by hydrothermal treatment of the $Na_xV_2O_5$ and GO. Then, the freestanding $Na_xV_2O_5$/rGO paper was obtained by facile vacuum filtration. The crystal structures of the as-synthesized samples ($Na_xV_2O_5$ and $Na_xV_2O_5$/rGO) are characterized by X-Ray diffraction (XRD). As shown in **Figure 2**, the XRD patterns of the synthesized $Na_xV_2O_5$ can be matched with a pure bilayer δ-$Na_xV_2O_5$ phase, which is consistent with previously reported results (Feng et al., 2018). $Na_xV_2O_5$/rGO exhibits similar diffraction patterns compared to that of the $Na_xV_2O_5$ sample, indicating $Na_xV_2O_5$ still exhibits high phase purity and GO has no effect on the formation of $Na_xV_2O_5{\cdot}nH_2O$ after the GO is added into the hydrothermal process. Then, the sodium to vanadium ratio was determined for the as-synthesized $Na_xV_2O_5$ sample by use of inductively coupled plasma optical emission spectroscopy (ICP-OES). The Na to V ratios in $Na_xV_2O_5$ samples were determined to be 0.16. When the vanadium level in each formula is set equal to 2.0, the corresponding sodium level in the $Na_xV_2O_5$ samples equals 0.32. (**Supplementary Table S1**). To confirm the morphology, SEM and TEM images were recorded on the as-synthesized $Na_xV_2O_5$ and $Na_xV_2O_5$/rGO paper. As shown in **Figure 3A**, one can see that the as-prepared $Na_xV_2O_5$ shows a long nanobelt morphology with a smooth surface and tens of micrometers in length and about 100–200 nm in width. The detailed crystal structures of $Na_xV_2O_5$ nanobelts were further characterized by a transmission electron microscope (TEM) (**Figures 3B,C**). The low-magnification TEM image (**Figure 3B**) further confirmed that the as-synthesized $Na_xV_2O_5$ nanobelts have a nanobelt structure, which is consistent with the observation in the SEM images. The high resolution (HR) TEM image demonstrates that these nanobelts are single crystals with an interplanar spacing of 0.36 nm, which corresponds to the (110) plane of the monoclinic phase $Na_xV_2O_5$ (**Figure 3C**). A typical scanning TEM image of a single $Na_xV_2O_5$ nanobelt and the corresponding element mapping images are recorded to further investigate the elemental distribution of the $Na_xV_2O_5$ nanobelt (**Figure 3D**). The elements Na, V, and O are homogeneously dispersed in the $Na_xV_2O_5$ nanobelt. **Figures 3E,F** exhibit the typical SEM images of $Na_xV_2O_5$/rGO paper. The interconnected $Na_xV_2O_5$ and rGO networks were observed, indicating the uniform intimate contact between $Na_xV_2O_5$ and rGO, which could increase the mechanical strength of freestanding $Na_xV_2O_5$/rGO hybrid paper to enhance cycling performance. **Figures 3G–I** shows optical images of freestanding $Na_xV_2O_5$/rGO paper, which can exhibit the excellent flexibility of $Na_xV_2O_5$/rGO paper and no obvious cracks were observed at the different bending states. Interestingly, based on the practical requirement, the

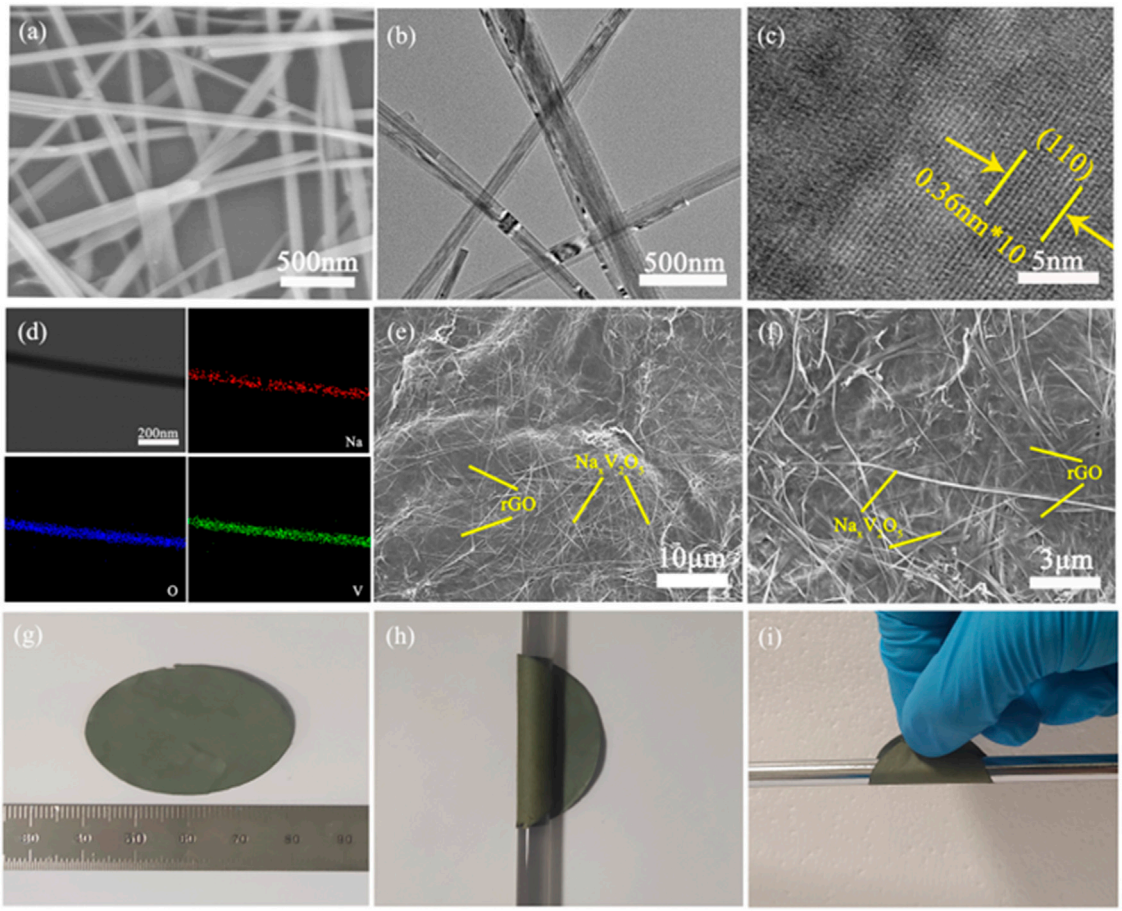

FIGURE 3 | (A) SEM of as-synthesized $Na_xV_2O_5$ powder;**(B)** TEM; **(C)** SAED; **(D)** EDS spectrum and Na, V, and O concentration in the $Na_xV_2O_5$ nanobelts. **(E,F)** SEM images of $Na_xV_2O_5$/rGO film; **(G–I)** Optical images of $Na_xV_2O_5$/rGO film at different bending states.

as-fabricated $Na_xV_2O_5$/rGO paper can be easily cut into the desired shapes to be directly used as the electrode of flexible SIBs.

To study the electrochemical performance of $Na_xV_2O_5$/rGO paper as cathode material for SIBs, the cyclic voltammetry (CV) test of $Na_xV_2O_5$/rGO nanocomposite electrode was first assessed during the initial three cycles at 0.1 mV s^{-1} (**Figure 4A**). The CV curves of $Na_xV_2O_5$/rGO are overlapping, suggesting the highly reversible electrochemical behaviors. The slightly different shape between the first CV curve and subsequent CV curves may be caused by the electrode polarization. Furthermore, It exhibits six main anodic current peaks around 1.91, 2.75, 2.82, 3.01, 3.15, and 3.65 V (vs. Na^+/Na), respectively, and six cathodic peaks around 1.65, 2.75, 2.91, 3.12, and 3.50 V (vs. Na^+/Na). The multiple redox peaks correspond to the multi-step insertion/extraction of Na^+ in the different available locations with energy differences. Two oxidation peaks (1.91 and 3.65 V) and reduction peaks (1.65 and 3.50 V) with high peak current demonstrate high Na + diffusion kinetics of the $Na_xV_2O_5$/rGO paper electrode. The cycling profiles of the $Na_xV_2O_5$/rGO electrode at 100 mA g^{-1} in the voltage range of 1.5–4.1 V are depicted in **Figure 4B**. The $Na_xV_2O_5$/rGO paper electrode shows analogous profiles corresponding well to the redox peaks of CV curves, indicating the good reversibility of the as-fabricated electrode. The dominated discharge/charge plateaus at about 3.6 V attributed to the reduction of V^{5+} to V^{4+} indicate a high electrochemical activity of V^{4+}/V^{5+}(He et al., 2016; Feng et al., 2018).

The cycling performance of $Na_xV_2O_5$/rGO paper as cathode materials for SIBs is further studied, as shown in **Figure 4C**. The cyclability of the $Na_xV_2O_5$/rGO paper electrode was first tested at a low current density of 100 mA g^{-1} (**Figure 4C**). It can deliver an initial charge/discharge capacity of 84 mAh g^{-1}/197 mAh g^{-1}. In the second and third cycles, the discharge capacity was almost no decay, demonstrating good Na-storage reversibility. After 150 cycles, a discharge specific capacity of 181 mAh g^{-1} was retained with a high capacity retention of 91% compared with that in the 1st cycle (**Figure 4C**). On the contrary, the $Na_xV_2O_5$ electrode exhibit degraded electrochemical performance. The first discharge capacity of the $Na_xV_2O_5$ electrode could reach 185 mAh g^{-1}, but the discharge capacity was only retained at 131 mAh g^{-1} after 150 cycles with a capacity retention of 70%. EIS tests are investigated to study the electrode reaction kinetics. **Supplementary Figures S1A,B**, the semicircle in high frequency (interfacial impedance, Rf) and middle frequency (charge transfer

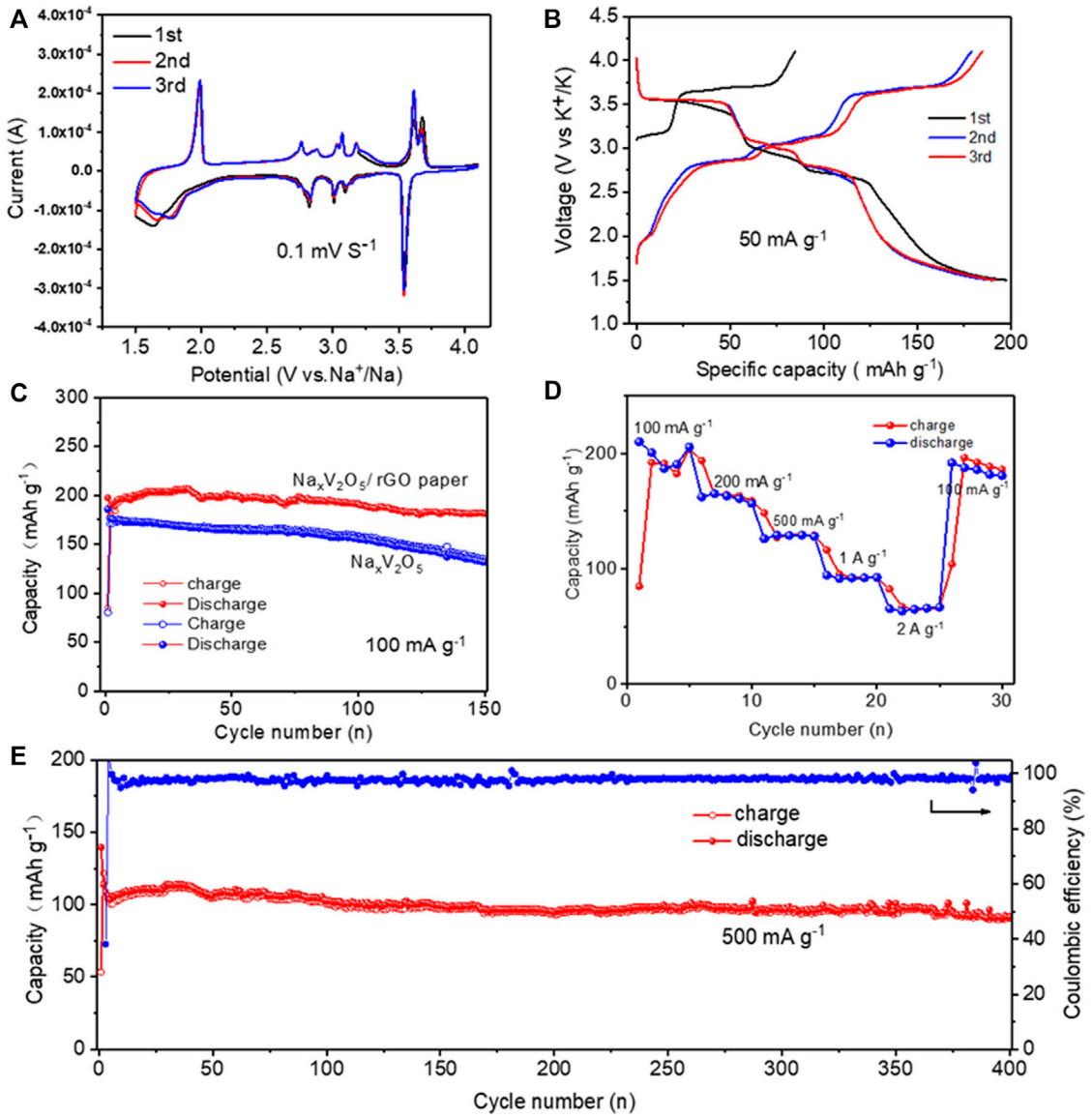

FIGURE 4 | (A) The initial three CV curves of the $Na_xV_2O_5$/rGO electrode at a scanning rate of 0.1 mV s^{-1}; **(B)** Initial three charge/discharge curves of the $Na_xV_2O_5$/rGO electrode at a current density of 100 mA g^{-1}. The electrochemical performance of $Na_xV_2O_5$/rGO electrode: **(C)** cycling performance; and **(D)** rate capability. **(E)** Cycling performance of $Na_xV_2O_5$/rGO electrode at a current density of 500 mAg^{-1}.

impedance, Rct) become larger after 10 cycles for $Na_xV_2O_5$ and $Na_xV_2O_5$/rGO. An equivalent circuit model was established, as shown in **Supplementary Figure S1**, where Rs is the internal resistance, Rf is the interfacial impedance, Rct represents the charge transfer resistance. As listed in **Supplementary Table S2**, the cycled NaxV2O5/rGO shows lower Rf and Rct than those of $Na_xV_2O_5$, indicating faster reaction kinetics of $Na_xV_2O_5$/rGO.

From the above results, the $Na_xV_2O_5$/rGO paper electrochemical showed superior cycling stability and strengthened reaction kinetics compared with the rare $Na_xV_2O_5$ electrodes. The rate performance of the $Na_xV_2O_5$/rGO paper at different current densities is shown in **Figure 4D**. The $Na_xV_2O_5$/rGO paper cathodes could exhibit average specific discharge capacities of 200, 163, 129, 92, and 65 mAh g^{-1} at current densities of 100, 200, 500, 1000, and 2000 mA g^{-1}, respectively. When the current density comes back to 100 mA g^{-1}, an average specific discharge capacity of 187 mAh g^{-1} could be preserved, showing the excellent electrochemical performance of the $Na_xV_2O_5$/rGO paper electrode at the different current densities. Considering the high reversibility of the as-prepared $Na_xV_2O_5$/rGO paper electrodes, we further evaluated the $Na_xV_2O_5$/rGO electrode at 500 mA g^{-1} for 400 cycles as shown in **Figure 4E**. A specific discharge capacity of 91 mAh g^{-1} was retained after 400 cycles with a capacity retention of 81%. Therefore, we believe the as-prepared $Na_xV_2O_5$/rGO paper electrodes exhibited a high rate

TABLE 1 | Comparison of the electrochemical performance of the electrode materials between this work and previous reports.

Materials	Operating voltage (V)	Initial discharge capacity (mAh g^{-1})	Capacity retention	Reference
$Na_xV_2O_5$/rGO	1.5–4.1	197 at 100 mA g^{-1}	91% (150 cycles)	
(this work)		113 at 500 mA g^{-1}	81% (400 cycles)	
NaV_3O_8	1.5–4.0	128 at 80 mA g^{-1}	77% (60 cycles)	(Kang et al., 2015)
$Na_xV_2O_5$/KB	1.5–4.0	109 at 200 mA g^{-1}	91% (100 cycles)	(Feng et al., 2018)
γ-$Na_{0.96}V_2O_5$	1.75–4.0	125 at 0.2°C	89% (50 cycles)	(Emery et al., 2018)
rGO/NaV_6O_{15}	1.5–3.8	150 at 100 mA g^{-1}	72% (50 cycles)	(Shang et al., 2019)
NaV_6O_{15}	1.5–4.0	126 at 100 mA g^{-1}	98% (100 cycles)	(Dong et al., 2020)

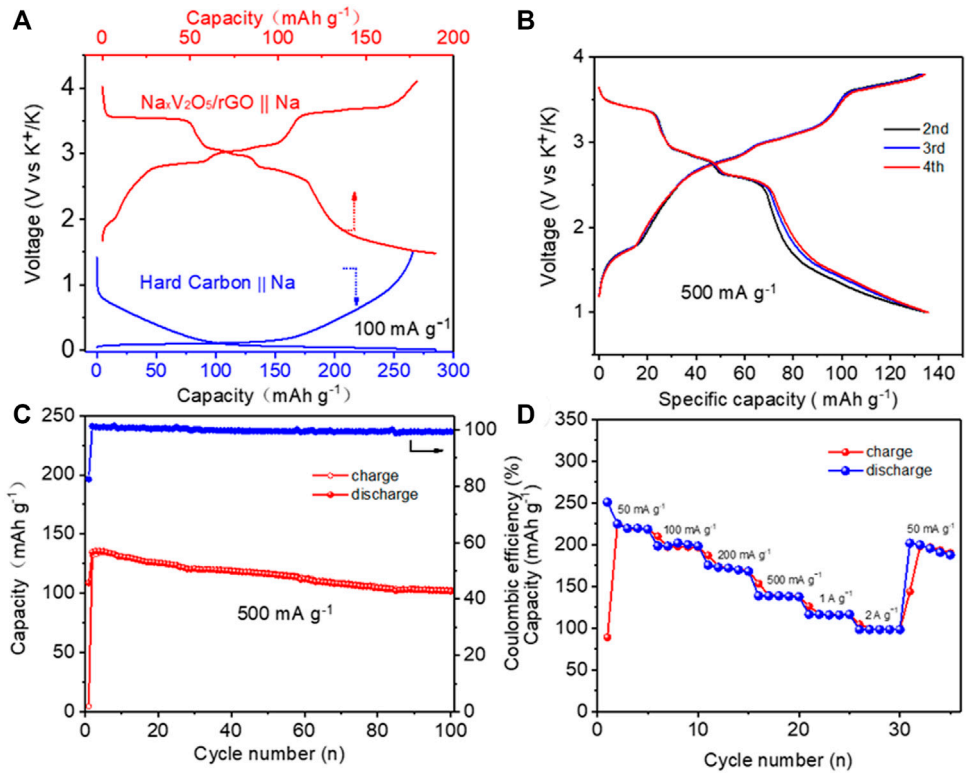

FIGURE 5 | Demonstration of SIBs based on $Na_xV_2O_5$/rGO || hard carbon configuration. **(A)** Typical charge–discharge curves of $Na_xV_2O_5$/rGO film || Na and hard carbon || Na in a half-cell configuration; **(B)** Electrochemical charge–discharge voltage profiles of SIBs, cycled at a current rate of 500 mA g^{-1}; **(C)** Cycling performance of SIBs at a constant current of 500 mA g^{-1}; **(D)** Rate capability of SIBs at different current rates, increasing from 50 mA g^{-1} to 2A g^{-1}.

performance and good cycling stability, indicating the enhanced electrochemical performance of the freestanding electrodes in the present work. To confirm the benefits of the $Na_xV_2O_5$/rGO paper, a comparison of the Na-storage performance between the as-prepared $Na_xV_2O_5$/rGO and other vanadium-based cathode materials is listed in **Table 1**. The electrochemical performance of our synthesized $Na_xV_2O_5$/rGO is superior to the vanadium-based cathode materials of SIBs recently reported. The good electrochemical performance of our $Na_xV_2O_5$/rGO films may be due to the following reasons: first, the bilayered $Na_xV_2O_5$ nanobelts with a large interlayer spacing and 1D belt-shaped morphology can reduce diffusion distance and provide a small diffusion for fast Na^+ ion insertion/extraction reactions. The other is that the presence of rGO can reduce the aggregation of $Na_xV_2O_5$ nanobelts and improve the conductivity of the whole composite material, which can strengthen the mechanical integrity of the composite and thus improve the cycling stability of the electrode.

Due to the high chemical activity of Na metal, the metallic Na anode would be highly dangerous in practical application. Na-ion full batteries based on hard carbon and $Na_xV_2O_5$/rGO paper as the anode and cathode electrodes, respectively, were assembled to further study the electrochemical behavior of full SIBs. **Figure 5A** depicts the typical voltage profiles of the hard carbon anode and $Na_xV_2O_5$/rGO paper cathode measured in the Na half-cell. Both the $Na_xV_2O_5$/rGO and hard carbon could achieve

reversible Na-ion transport from their respective skeleton structures. **Figure 5B** shows the charge–discharge profiles of the full battery at 500 mA g^{-1} with cut-off voltages of 3.8 and 1.0 V. The initial discharge-specific capacities could attain 109 mAh g^{-1}. Charge-discharge specific capacities could also retain 134/135 mAh g^{-1} with a high Coulombic efficiency of 99% in the second cycle. As shown in **Figure 5C**, after 100 cycles, the full Na-ion battery retained a discharge specific capacity of 101 mAh g^{-1} with a capacity retention of >75%, showing the good cycling performance of SIBs based on $Na_xV_2O_5$/rGO paper electrode and hard carbon electrode. Importantly, the average Coulombic efficiency was higher than 98% during the 100 cycles, suggesting the highly reversible Na-ion storage behavior for the full Na-ion battery. Besides the high capacity retention, the full Na-ion battery also exhibited a good rate of performance. As shown in **Figure 5D**, the full Na-ion battery delivered average specific discharge capacities of 218, 197, 172, 137, 113, and 97 mAh g^{-1} at constant current densities of 50, 100, 200, 500, 1000, and 2000 mA g^{-1} respectively. When the current density was recovered to 50 mA g^{-1}, the reversible capacity came back to 193 mAh g^{-1}, indicating a good tolerance for the rapid Na-ion insertion/extraction cycles. The current work shows that the $Na_xV_2O_5$/rGO has great potential as the freestanding cathode material for stable sodium ion batteries.

CONCLUSION

In summary, a flexible $Na_xV_2O_5$/rGO paper was successfully prepared *via* the hydrothermal method followed by vacuum filtration as a high-performance cathode for SIBs. The as-prepared $Na_xV_2O_5$/rGO possessed flexibility and high conductivity that can buffer stress and facilitate the fast transportation of electrons during the charge-discharge process. As a result, the as-prepared $Na_xV_2O_5$-rGO paper can deliver a reversible Na-ion storage capacity of ~197 mA h g^{-1} at 100 mA g^{-1} and showed a good cycling performance with 81% capacity retention for 400 cycles at a high current density of 500 mA g^{-1}, showing great potentials in flexible energy storage devices.

DATA AVAILABILITY STATEMENT

The original contributions presented in the study are included in the article/**Supplementary Material**, further inquiries can be directed to the corresponding author.

AUTHOR CONTRIBUTIONS

JX conceived the concept and directed the research. QW and XL designed the project. QW and XL carried out material synthesis. YY and XYL performed material characterization. JX and XW wrote the paper. All authors discussed the results and commented on the paper.

FUNDING

This work was supported by the Students' Innovation and Entrepreneurship Training Program of Zhengzhou University (No.2020cxcy101).

SUPPLEMENTARY MATERIAL

The Supplementary Material for this article can be found online at: https://www.frontiersin.org/articles/10.3389/fmats.2022.913804/full#supplementary-material

REFERENCES

Baddour-Hadjean, R., Safrany Renard, M., Emery, N., Huynh, L. T. N., Le, M. L. P., and Pereira-Ramos, J. P. (2018). The Richness of V2O5 Polymorphs as Superior Cathode Materials for Sodium Insertion. *Electrochimica Acta* 270, 129–137. doi:10.1016/j.electacta.2018.03.062

Córdoba, R., Kuhn, A., Pérez-Flores, J. C., Morán, E., Gallardo-Amores, J. M., and García-Alvarado, F. (2019). Sodium Insertion in High Pressure β-V2O5: A New High Capacity Cathode Material for Sodium Ion Batteries. *J. Power Sources* 422, 42–48. doi:10.1016/j.jpowsour.2019.03.018

Dong, Y., Xu, J., Chen, M., Guo, Y., Zhou, G., Li, N., et al. (2020). Self-assembled NaV6O15 Flower-like Microstructures for High-Capacity and Long-Life Sodium-Ion Battery Cathode. *Nano Energy* 68, 104357. doi:10.1016/j.nanoen.2019.104357

Emery, N., Baddour-Hadjean, R., Batyrbekuly, D., Laïk, B., Bakenov, Z., and Pereira-Ramos, J.-P. (2018). γ-Na0.96V2O5: A New Competitive Cathode Material for Sodium-Ion Batteries Synthesized by a Soft Chemistry Route. *Chem. Mat.* 30 (15), 5305–5314. doi:10.1021/acs.chemmater.8b02066

Feng, J., Xiong, Z., Zhao, L., Huang, C., Liu, H., Chen, S., et al. (2018). One-pot Hydrothermal Synthesis of NaxV2O5·nH2O/KB Nanocomposite as a Sodium-Ion Battery Cathode for Improved Reversible Capacity and Rate Performance. *J. Power Sources* 396, 230–237. doi:10.1016/j.jpowsour.2018.06.021

Guignard, M., Didier, C., Darriet, J., Bordet, P., ElkaïmDelmas, E. C., and Delmas, C. (2013). P2-NaxVO2 System as Electrodes for Batteries and Electron-Correlated Materials. *Nat. Mater* 12 (1), 74–80. doi:10.1038/nmat3478

He, G., Kan, W. H., and Manthiram, A. (2016). A 3.4 V Layered VOPO4 Cathode for Na-Ion Batteries. *Chem. Mat.* 28 (2), 682–688. doi:10.1021/acs.chemmater.5b04605

Huang, H., Xu, R., Feng, Y., Zeng, S., Jiang, Y., Wang, H., et al. (2020). Sodium/Potassium-Ion Batteries: Boosting the Rate Capability and Cycle Life by Combining Morphology, Defect and Structure Engineering. *Adv. Mat.* 32 (8), 1904320. doi:10.1002/adma.201904320

Huang, J., Wei, Z., Liao, J., Ni, W., Wang, C., and Ma, J. (2019). Molybdenum and Tungsten Chalcogenides for Lithium/sodium-Ion Batteries: Beyond MoS2. *J. Energy Chem.* 33, 100–124. doi:10.1016/j.jechem.2018.09.001

Huang, T., Niu, Y., Yang, Q., Yang, W., and Xu, M. (2021). Self-Template Synthesis of Prussian Blue Analogue Hollow Polyhedrons as Superior Sodium Storage Cathodes. *ACS Appl. Mat. Interfaces* 13 (31), 37187–37193. doi:10.1021/acsami.1c09678

Jiang, Y., Hu, M., Zhang, D., Yuan, T., Sun, W., Xu, B., et al. (2014). Transition Metal Oxides for High Performance Sodium Ion Battery Anodes. *Nano Energy* 5, 60–66. doi:10.1016/j.nanoen.2014.02.002

Jo, J. H., Choi, J. U., Park, Y. J., Ko, J. K., Yashiro, H., and Myung, S.-T. (2020). A New Pre-sodiation Additive for Sodium-Ion Batteries. *Energy Storage Mater.* 32, 281–289. doi:10.1016/j.ensm.2020.07.002

Kang, H., Liu, Y., Shang, M., Lu, T., Wang, Y., and Jiao, L. (2015). NaV3O8 Nanosheet@polypyrrole Core-Shell Composites with Good Electrochemical

Performance as Cathodes for Na-Ion Batteries. *Nanoscale* 7 (20), 9261–9267. doi:10.1039/c5nr02064f

Li, S., Dong, Y., Xu, L., Xu, X., He, L., and Mai, L. (2014). Effect of Carbon Matrix Dimensions on the Electrochemical Properties of Na3V2(PO4)3Nanograins for High-Performance Symmetric Sodium-Ion Batteries. *Adv. Mat.* 26 (21), 3545–3553. doi:10.1002/adma.201305522

Li, X., Fu, J., Sun, Y., Sun, M., Cheng, S., Chen, K., et al. (2019). Design and Understanding of Core/branch-Structured VS2 nanosheets@CNTs as High-Performance Anode Materials for Lithium-Ion Batteries. *Nanoscale* 11 (28), 13343–13353. doi:10.1039/c9nr03581h

Li, X., Zhuang, C., Xu, J., Li, L., Xu, T., Dai, S., et al. (2021). Rational Construction of K0.5V2O5 nanobelts/CNTs Flexible Cathode for Multi-Functional Potassium-Ion Batteries. *Nanoscale* 13 (17), 8199–8209. doi:10.1039/d1nr00993a

Liang, J., Wei, Z., Wang, C., and Ma, J. (2018). Vacancy-induced Sodium-Ion Storage in N-Doped Carbon Nanofiber@MoS2 Nanosheet Arrays. *Electrochimica Acta* 285, 301–308. doi:10.1016/j.electacta.2018.07.230

Lim, S. Y., Kim, H., Chung, J., Lee, J. H., Kim, B. G., Choi, J.-J., et al. (2014). Role of Intermediate Phase for Stable Cycling of Na 7 V 4 (P 2 O 7) 4 PO 4 in Sodium Ion Battery. *Proc. Natl. Acad. Sci. U.S.A.* 111 (2), 599–604. doi:10.1073/pnas.1316557110

Liu, Q., Hu, Z., Chen, M., Zou, C., Jin, H., Wang, S., et al. (2020a). The Cathode Choice for Commercialization of Sodium-Ion Batteries: Layered Transition Metal Oxides versus Prussian Blue Analogs. *Adv. Funct. Mat.* 30 (14), 1909530. doi:10.1002/adfm.201909530

Liu, Y., He, D., Cheng, Y., Li, L., Lu, Z., Liang, R., et al. (2020b). A Heterostructure Coupling of Bioinspired, Adhesive Polydopamine, and Porous Prussian Blue Nanocubics as Cathode for High-Performance Sodium-Ion Battery. *Small* 16 (11), 1906946. doi:10.1002/smll.201906946

Lu, J., Chen, Z., Ma, Z., Pan, F., Curtiss, L. A., and Amine, K. (2016). The Role of Nanotechnology in the Development of Battery Materials for Electric Vehicles. *Nat. Nanotech* 11 (12), 1031–1038. doi:10.1038/nnano.2016.207

Ma, C., Xu, T., Yan, C., Xu, J., Kong, D., Zhang, Z., et al. (2021). Mechanism Investigation of High Performance Na3V2(PO4)2O2F/reduced Graphene Oxide Cathode for Sodium-Ion Batteries. *J. Power Sources* 482, 228906. doi:10.1016/j.jpowsour.2020.228906

Niu, Y., Zhang, Y., and Xu, M. (2019). A Review on Pyrophosphate Framework Cathode Materials for Sodium-Ion Batteries. *J. Mat. Chem. A* 7 (25), 15006–15025. doi:10.1039/c9ta04274a

Osman, S., Zuo, S., Xu, X., Shen, J., Liu, Z., Li, F., et al. (2021). Freestanding Sodium Vanadate/Carbon Nanotube Composite Cathodes with Excellent Structural Stability and High Rate Capability for Sodium-Ion Batteries. *ACS Appl. Mat. Interfaces* 13 (1), 816–826. doi:10.1021/acsami.0c21328

Pei, Z., Li, H., Huang, Y., Xue, Q., Huang, Y., Zhu, M., et al. (2017). Texturing *In Situ*: N,S-enriched Hierarchically Porous Carbon as a Highly Active Reversible Oxygen Electrocatalyst. *Energy Environ. Sci.* 10 (3), 742–749. doi:10.1039/c6ee03265f

Qu, J., Bai, Y., Li, X., Song, K., Zhang, S., Wang, X., et al. (2021). Rational Design of NiSe2@rGO Nanocomposites for Advanced Hybrid Supercapacitors. *J. Mater. Res. Technol.* 15, 6155–6161. doi:10.1016/j.jmrt.2021.11.036

Senthilkumar, B., Rambabu, A., Murugesan, C., Krupanidhi, S. B., and Barpanda, P. (2020). Iron-Based Mixed Phosphate Na4Fe3(PO4)2P2O7 Thin Films for Sodium-Ion Microbatteries. *ACS Omega* 5 (13), 7219–7224. doi:10.1021/acsomega.9b03835

Shang, C., Hu, L., Lin, Q., Fu, X., Wang, X., and Zhou, G. (2019). Integration of NaV6O15·nH2O Nanowires and rGO as Cathode Materials for Efficient Sodium Storage. *Appl. Surf. Sci.* 494, 458–464. doi:10.1016/j.apsusc.2019.07.192

Venkatesh, G., Pralong, V., Lebedev, O. I., Caignaert, V., Bazin, P., and Raveau, B. (2014). Amorphous Sodium Vanadate Na1.5+yVO3, a Promising Matrix for Reversible Sodium Intercalation. *Electrochem. Commun.* 40, 100–102. doi:10.1016/j.elecom.2013.11.004

Wang, Y., Lim, Y. V., Huang, S., Ding, M., Kong, D., Pei, Y., et al. (2020). Enhanced Sodium Storage Kinetics by Volume Regulation and Surface Engineering via Rationally Designed Hierarchical Porous FeP@C/rGO. *Nanoscale*, 12 (7), 4341–4351. doi:10.1039/c9nr09278a

Wu, L., Lu, H., Xiao, L., Qian, J., Ai, X., Yang, H., et al. (2014). A Tin(ii) Sulfide-Carbon Anode Material Based on Combined Conversion and Alloying Reactions for Sodium-Ion Batteries. *J. Mat. Chem. A* 2 (39), 16424–16428. doi:10.1039/c4ta03365e

Xu, G., Liu, X., Huang, S., Li, L., Wei, X., Cao, J., et al. (2020). Freestanding, Hierarchical, and Porous Bilayered NaxV2O5·nH2O/rGO/CNT Composites as High-Performance Cathode Materials for Nonaqueous K-Ion Batteries and Aqueous Zinc-Ion Batteries. *ACS Appl. Mat. Interfaces* 12 (1), 706–716. doi:10.1021/acsami.9b17653

Xu, J., Dou, S., Liu, H., and Dai, L. (2013). Cathode Materials for Next Generation Lithium Ion Batteries. *Nano Energy* 2 (4), 439–442. doi:10.1016/j.nanoen.2013.05.013

Xu, J., Tang, H., Xu, T., Wu, D., Shi, Z., Tian, Y., et al. (2017). Porous NiO Hollow Quasi-Nanospheres Derived from a New Metal-Organic Framework Template as High-Performance Anode Materials for Lithium Ion Batteries. *Ionics* 23, 3273–3280. doi:10.1007/s11581-017-2160-4

Zhao, H., Zhuang, C., Xu, J., Zhang, Z., Shen, W., Tang, H., et al. (2020). Synergistically Enhanced Sodium/potassium Ion Storage Performance of SnSb Alloy Particles Confined in Three-Dimensional Carbon Framework. *Ionics* 26 (10), 5019–5028. doi:10.1007/s11581-020-03641-2

Zhou, W., Chen, J., He, C., Chen, M., Xu, X., Tian, Q., et al. (2019). Hybridizing δ-type NaxV2O5·nH2O with Graphene towards High-Performance Aqueous Zinc-Ion Batteries. *Electrochimica Acta* 321, 134689. doi:10.1016/j.electacta.2019.134689

Zhu, Y.-H., Zhang, Q., Yang, X., Zhao, E.-Y., Sun, T., Zhang, X.-B., et al. (2019). Reconstructed Orthorhombic V2O5 Polyhedra for Fast Ion Diffusion in K-Ion Batteries. *Chem* 5 (1), 168–179. doi:10.1016/j.chempr.2018.10.004

Conflict of Interest: The authors declare that the research was conducted in the absence of any commercial or financial relationships that could be construed as a potential conflict of interest.

Publisher's Note: All claims expressed in this article are solely those of the authors and do not necessarily represent those of their affiliated organizations, or those of the publisher, the editors and the reviewers. Any product that may be evaluated in this article, or claim that may be made by its manufacturer, is not guaranteed or endorsed by the publisher.